RSC Advances

RSC Publishing

PAPER

View Article Online
View Journal | View Issue

Coral-like V_2O_5 nanowhiskers as high-capacity cathode materials for lithium-ion batteries

Cite this: *RSC Advances*, 2013, **3**, 5069

Bei Wang,*[a] Ying Wang,[a] Bing Sun,[a] Paul Munroe[b] and Guoxiu Wang*[a]

Received 7th October 2012,
Accepted 4th February 2013

DOI: 10.1039/c3ra22425b

www.rsc.org/advances

Coral-like V_2O_5 nanowhiskers were prepared by a direct electrolytic synthesis method. The as-prepared V_2O_5 nanowhiskers are approximately 1 μm in length and 50–60 nm in width, which was confirmed by scanning electron microscopy and transmission electron microscopy analysis. When applied as cathode materials in lithium-ion batteries and combined with an ionic liquid electrolyte, the V_2O_5 nanowhiskers exhibited an initial capacity of 461 mAh g^{-1}, which is a significant enhancement compared to commercial V_2O_5 powders. The high rate performance of the V_2O_5 nanowhiskers was further improved at an elevated working temperature of 50 °C. The V_2O_5 nanowhiskers demonstrated a high specific capacity and an excellent high-rate performance at elevated temperatures.

Introduction

To meet the critical requirement of energy demand and to address global warming and climate change, reliable green energy storage devices have been developed over the last few decades.[1,2] The second generation lithium-ion batteries can provide high energy density and long service life for many applications.[3–5] By applying nanosized electroactive materials, the electrochemical performances of lithium-ion cells can be enhanced. Typical electrode materials, such as $LiFePO_4$,[6,7] elemental sulfur,[8–10] and transition metal oxides,[4] have been intensively studied to improve their electrochemical properties. However, it is still a challenge to develop optimized combinations of high-performance active materials and compatible electrolytes for lithium-ion batteries.[5]

Among all potential electrode materials, V_2O_5 is considered as a promising cathode candidate, owing to its high theoretical capacity (437 mAh g^{-1}) and low cost. Various V_2O_5 nanostructures have been used in lithium-ion batteries, including one-dimensional nanorods,[11] nanoribbons,[12] nanowires,[12] nanotubes,[13–15] nanobelts/nanorolls,[16] hollow microspheres from nanorods,[17] and mesoporous structures.[18] They demonstrated improved electrochemical performance, attributed to the short paths for lithium-ion diffusion. Electrochemical electrolytic processes have been reported to synthesize V_2O_5 microstructures.[19–21]

In this paper, we report a direct synthesis of coral-like V_2O_5 nanowhiskers by a simple electrolytic process. The electrochemical conditions of the electrolytic process have been optimized. Coral-like V_2O_5 nanowhiskers were obtained by removing the hydrated water from the $V_2O_5{\cdot}xH_2O$ precursor. Combined with an ionic liquid electrolyte, V_2O_5 nanowhiskers exhibited higher specific capacities and better prolonged cycling stability than those of commercial V_2O_5 powders. Electrochemical performance at high current rates was further improved at an elevated working temperature of 50 °C.

Experimental

In a typical synthesis process, 3.26 g $VOSO_4{\cdot}xH_2O$ was dissolved in 100 ml deionized water, followed by the addition of 0.5 M H_2SO_4 solution to adjust the pH to 2. The solution was then taken for electrolytic treatment with two noble platinum electrodes at 80 °C for 2 h. The working voltage was set to 2 V against a Saturated Calomel Electrode (SCE). The yellow green precipitates formed during the electrolytic process were collected, washed with abundant water and ethanol, and finally dried at 60 °C in a vacuum oven overnight. The dried precipitates were further sintered at 400 °C for 2 h in air to obtain the final product.

X-ray diffraction (XRD) patterns of the precursor prior to calcination and the as-synthesized material were measured using a Siemens D5000 X-ray diffractometer from 5° to 60° under a scan rate of 1° min^{-1}. Field-emission scanning electron microscope (FESEM) observations were performed using a Zeiss Supra 55 VP FESEM with an Oxford energy dispersive spectrometry system. Transmission electron microscopy (TEM) analysis was carried out using a JEOL 2011 TEM facility. N_2 adsorption-desorption isotherms of the V_2O_5 nanowhisker and commercial samples were obtained on a Tristar II analyzer at 77 K. The Brunauer–Emmett–Teller (BET)

[a]*Centre for Clean Energy Technology & School of Chemistry and Forensic Science, University of Technology Sydney, City Campus, Broadway, Sydney 2007, Australia. E-mail: Bei.Wang-1@student.uts.edu.au; Guoxiu.Wang@uts.edu.au; Fax: +61 2 95141460; Tel: +61 2 95141741*
[b]*Mark Wainwright Analytical Centre, University of New South Wales, Kensington 2052, Australia*

surface area was derived by using the experimental points at a relative pressure (P/P_0) of 0.05–0.25.

For electrochemical testing, the electrodes were fabricated by mixing 80 wt% V_2O_5 nanowhiskers, 10 wt% carbon black, and 10 wt% polyvinylidene fluoride binder in *N*-methyl-2-pyrrolidone solvent to form a slurry. The slurry was then coated on aluminum foil substrates. Lithium foils were used as the negative electrodes. CR2032 coin cells were assembled in an argon-filled glove box (Unilab, Germany), in which moisture and oxygen were controlled to be less than 0.1 ppm. The electrolyte was an ionic liquid (IL) prepared by 0.5 M lithium bis(trifluoromethanesulfonyl) imide ($LiNTf_2$) in *N*-methyl-*N*-propyl pyrrolidinium bis(trifluoromethanesulfonyl) imide ($[C_3mpyr][NTf_2]$). For comparison, conventional electrolyte (CE), 1 M $LiPF_6$ in ethylene carbonate and dimethyl carbonate (1 : 1), was also used to assemble the test cells. Cyclic voltammetry (CV) was carried out on an electrochemistry workstation (CHI660D) at a scan rate of 0.1 mV s^{-1} *vs.* Li/Li^+ reference electrode in the voltage range of 1.5 to 4 V. Galvanostatic charge/discharge measurements were conducted on a Neware battery tester with a current rate of 0.1 C (equivalent to 43.7 mA g^{-1}). Stepwise high-rate cycling performance was evaluated at current rates of 0.05, 0.1, 0.2, 0.5, 1 and 2 C and then back to 0.5 and 0.1 C. Electrochemical impedance spectroscopy was measured on the CHI660D electrochemistry workstation. The frequency was set in the range of 0.01 Hz–100 kHz with an amplitude of 5 mV. The charge/discharge cycling properties and the rate performance were also investigated for commercial V_2O_5 powders. Further observations on the V_2O_5 nanowhisker electrodes before cyclic testing and after 50 cycles in both IL and CE were carried out on the same FESEM facility as shown above. Fresh electrodes were directly examined as a reference while cycled electrodes were taken out from the cycled lithium cells, washed with acetone and dried thoroughly at 100 °C under vacuum prior to examination.

Results and discussion

Powder X-ray diffraction patterns of the precursor and the as-prepared product are shown in Fig. 1. The precursor is identified as vanadium oxide hydrate ($V_2O_5{\cdot}xH_2O$) (Fig. 1(a)). All indexed diffraction peaks are consistent with the previously reported result.[21] $V_2O_5{\cdot}xH_2O$ lost its hydrated water during thermal treatment and transformed to V_2O_5 as shown in Fig. 1(b). All the diffraction lines of the as-prepared V_2O_5 nanowhiskers are indexed to the orthorhombic crystal structure (Joint Committee on Powder Diffraction Standards (JCPDS) card 41-1426, Pnmm (59)).

Fig. 2 shows morphologies of the $V_2O_5{\cdot}xH_2O$ precursor, V_2O_5 nanowhiskers and commercial powders. Fig. 2(a) and (b) are the typical FESEM images of the precursor. The precursor ($V_2O_5{\cdot}xH_2O$) consists of microsheets formed from the electrolytic process. These sheets are a few micrometers in size and well-separated with wrinkled surfaces. During calcination, the

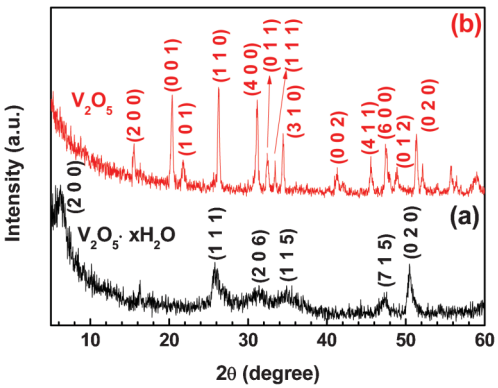

Fig. 1 XRD patterns of (a) $V_2O_5{\cdot}xH_2O$ precursor and (b) V_2O_5 nanowhiskers.

hydrated water was gradually removed from the surface of the $V_2O_5{\cdot}xH_2O$ microsheets, resulting in coral-like bundles of V_2O_5 nanowhiskers (as shown in Fig. 2(c) and (d)). It can be seen from Fig. 2(e) that the commercial V_2O_5 powders are non-uniform agglomerates of small particles, which are a few hundred nanometers in size, as visualized in Fig. 2(f). Fig. 3(a) shows a TEM image focusing on a single V_2O_5 nanowhisker with a length of approximately 1 μm and a width of about 50–60 nm. The corresponding Selected Area Electron Diffraction (SAED) is displayed as the inset in Fig. 3(a). Several diffraction dots are indexed to (7 1 0), (3 0 2), (1 1 4), (4 1 2) planes of crystalline V_2O_5 along the [2 14 3] zone axis. This further confirms the presence of high purity V_2O_5 phase. The high resolution TEM (HRTEM) image shows the well-resolved lattice

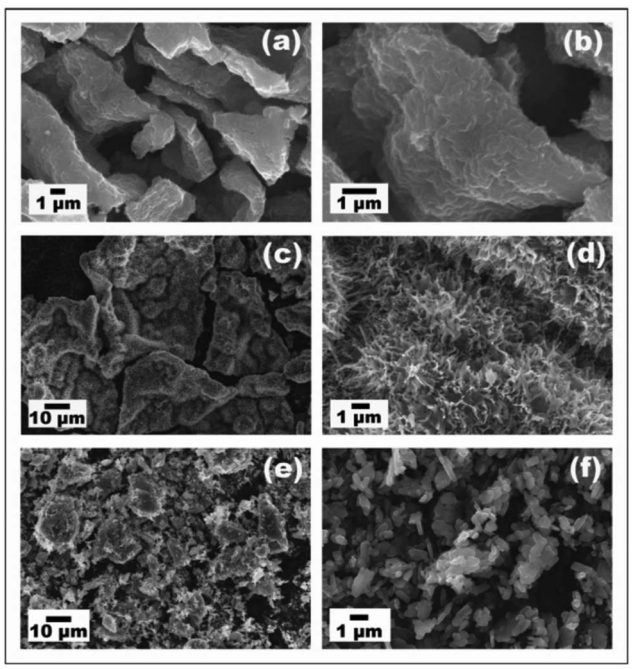

Fig. 2 FESEM images showing general morphologies of (a) and (b) the $V_2O_5{\cdot}xH_2O$ precursor, (c) and (d) the as-prepared V_2O_5 product, and (e) and (f) the commercial V_2O_5 powders.

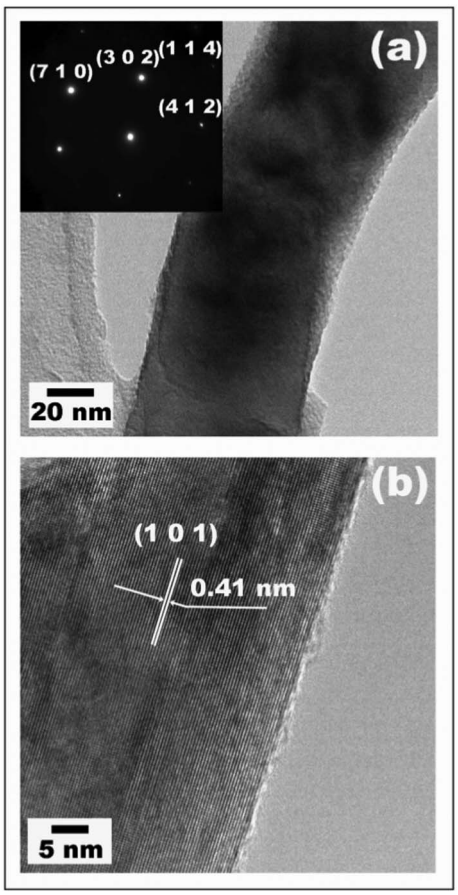

Fig. 3 TEM images focusing on a single V_2O_5 nanowhisker: (a) a low magnified image with its SAED pattern (inset), and (b) an HRTEM image with indexed (1 0 1) crystal planes.

fringe (Fig. 3(b)). The crystal lattice can be indexed to (1 0 1) with a *d*-spacing of 0.41 nm. TEM, SAED and HRTEM analysis clearly confirmed the single crystalline nature of individual V_2O_5 nanowhiskers. Unlike those previously reported agglomerates in micrometer size,[21] V_2O_5 nanowhiskers can provide a much shorter path for lithium-ion diffusion when applied as electrode materials in lithium-ion batteries.

The BET surface areas of both V_2O_5 nanowhiskers and commercial powders were derived from the N_2 adsorption and desorption isotherms, as shown in Fig. 4. The V_2O_5 nanowhisker sample has a high surface area of 28 m^2 g^{-1}, nine times larger than that of the V_2O_5 commercial powders (3 m^2 g^{-1}).

Cyclic voltammetry curves of the as-prepared V_2O_5 nanowhiskers with the IL electrolyte are shown in Fig. 5. In the first cycle, four reduction peaks can be identified, which are assigned to the transformations of V_2O_5 to different $Li_xV_2O_5$ phases upon lithium insertion,[22,23] where *x* represents the number of moles of the inserted lithium ions in per mol V_2O_5. At the voltage of ~1.87 V, a ω-$Li_xV_2O_5$ (x = 3) phase was irreversibly formed.[22] From the second cycle, the CV curves showed only broad redox peaks arising from the insertion/extraction of the lithium ions. The CV curves were then highly

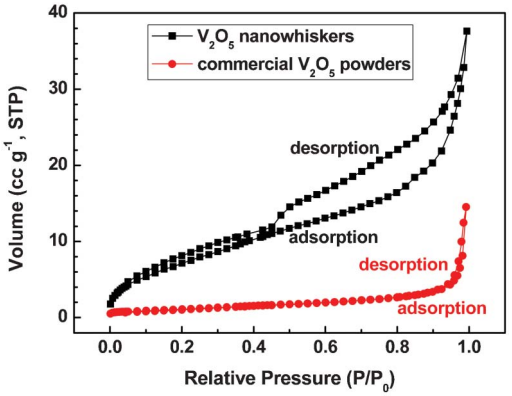

Fig. 4 N_2 adsorption–desorption isotherms of V_2O_5 nanowhiskers and commercial V_2O_5 powders.

overlapped from the 2nd cycle, indicating highly reversible lithium insertion/extraction processes.

The charge/discharge profiles of the as-prepared V_2O_5 nanowhiskers are shown in Fig. 6 with both IL and CE electrolytes at a current density of 0.1 C (equivalent to 43.7 mA g^{-1}). When the IL electrolyte was used (Fig. 6(a)), four voltage plateaux were identified in the 1st cycle, which are consistent with the four reduction peaks presented in the CV curves in Fig. 5. The highest specific discharge capacity achieved is 461 mAh g^{-1} in the 1st cycle. This high initial capacity could be attributed to the complete 3 mol Li^+ insertion per mole of V_2O_5, accompanying the transformation of V_2O_5 to the irreversible ω-$Li_xV_2O_5$ phase.[22] From the 2nd cycle, a reversible discharge capacity of 382 mAh g^{-1} was obtained and a stable capacity of 338 mAh g^{-1} retained in the 50th cycle. Similarly, the cell with the CE electrolyte also presented four voltage plateaux but with small voltage variations compared to the cell with the IL electrolyte. The discharge capacities obtained were 378, 318, 194 mAh g^{-1} in the 1st, 2nd, 50th cycles, respectively.

Long-term cycling investigation are shown in Fig. 7 for V_2O_5 nanowhiskers and commercial V_2O_5 powders with both IL and CE electrolytes at a current density of 0.1 C. The V_2O_5

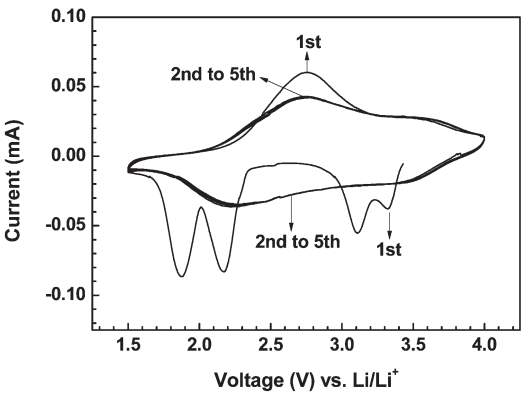

Fig. 5 CV curves of the V_2O_5 nanowhisker electrode with IL electrolyte at a sweep rate of 0.1 mV s^{-1} in the first 5 cycles.

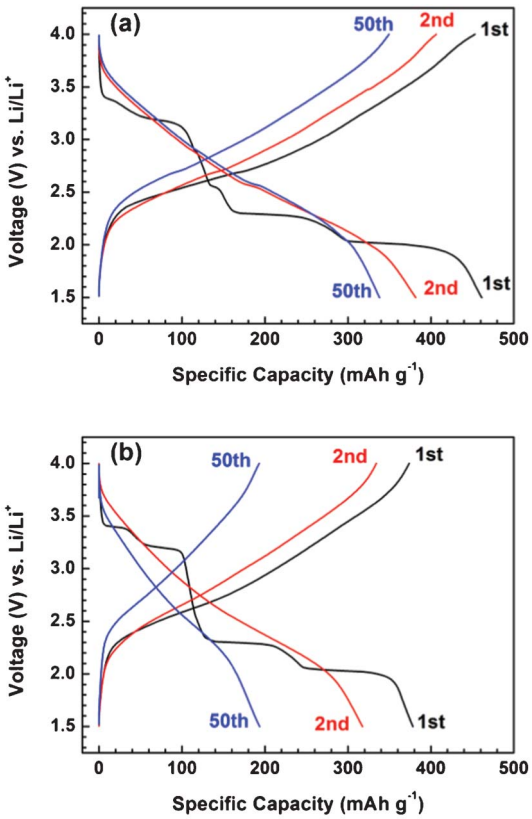

Fig. 6 Charge/discharge profiles of the V_2O_5 nanowhisker electrodes with electrolytes of (a) IL and (b) CE at a current density of 0.1 C (equivalent to 43.7 mA g^{-1}).

nanowhiskers combined with the IL electrolyte exhibited the highest specific capacity and most stable cycling performance. The initial capacity in the 1st cycle was 461 mAh g^{-1} and gradually reached a stable value of around 335 mAh g^{-1}. After 50 cycles, a final capacity of 338 mAh g^{-1} was maintained, showing a stable cyclability. Commercial V_2O_5 with the IL electrolyte performed second best, with a good cyclability for up to 50 cycles. On the contrary, both V_2O_5 nanowhiskers and commercial powders with the CE electrolyte showed decreased capacities upon cycling and quite low specific capacities. It should be noted that the V_2O_5 nanowhiskers delivered higher capacities by using the IL electrolyte, compared to that using the CE electrolyte and showed a much better capacity retention (338 *vs.* 194 mAh g^{-1}) after 50 cycles. It can also be seen that all the V_2O_5 electrodes showed higher specific capacities than $LiFePO_4$ (170 mAh g^{-1}) and $LiCoO_2$ (140 mAh g^{-1}). The advantages of employing ionic liquid electrolyte in lithium-ion batteries have been previously reported, including battery safety, electrochemical and thermal stability, and prevention of lithium dendrites.[24,25] Furthermore, the use of IL electrolyte can effectively prevent $LiNTf_2$ salts to corrode the aluminium substrates.[26] The combination of V_2O_5 and IL electrolyte (0.5 M $LiNTf_2$ in $[C_3mpyr][NTf_2]$) could significantly enhance the electrochemical performance of lithium-ion batteries, which has been proved by Chou *et al.*[12]

Fig. 8 shows the FESEM images of the V_2O_5 nanowhisker electrodes before cyclic tests and after 50 cycles in both IL and CE. It can be seen that the fresh electrode (Fig. 8(a) and (b)) has a flattened surface and a uniform structure. The electrode cycled in IL (Fig. 8(c) and (d)) presents similar microstructure as the fresh electrode, but with a slightly unflattened surface and a low degree of cracking. However, the whole structure of the electrode was well maintained during the cyclic test, and this would ensure a vital cycling performance. On the other hand, the electrode cycled in CE (Fig. 8(e) and (f)) exhibits severe cracks and caves. The surface of the electrode was no

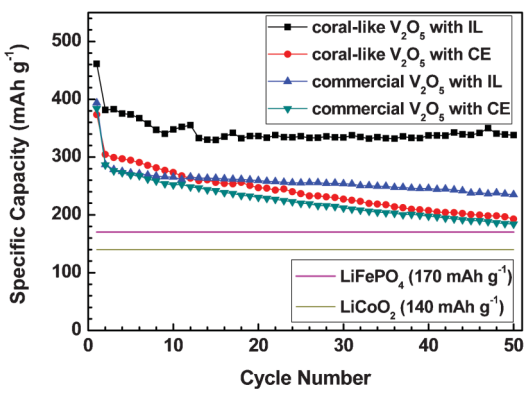

Fig. 7 Cycling performances of V_2O_5 nanowhiskers and commercial V_2O_5 powders with both IL and CE at room temperature (20 °C) for 50 cycles at a current density of 0.1 C.

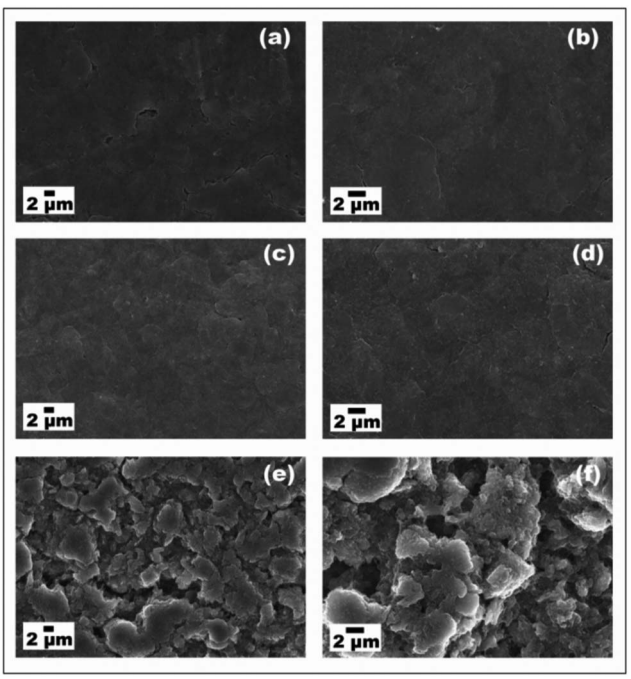

Fig. 8 FESEM images of V_2O_5 nanowhisker electrodes: (a) and (b) fresh electrode; (c) and (d) electrode after 50 cycles in IL; and (e) and (f) electrode after 50 cycles in CE.

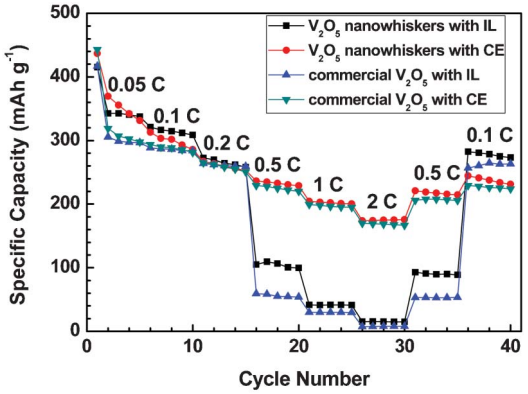

Fig. 9 Rate performances of V_2O_5 nanowhiskers and commercial V_2O_5 powders with both IL and CE at room temperature of 20 °C.

longer flattened and the structure was torn apart into smaller aggregates, indicating the dissolution of the V_2O_5 active material and the weight loss of the electrode. The almost destroyed electrode structure was the main reason for the quick capacity decay under prolonged cycling. Therefore, all these FESEM images provide indirect evidence of a better cycling stability of V_2O_5 electrodes by using IL as the electrolyte over CE.

Rate performance is a critical property of lithium-ion batteries in practical applications. Fig. 9 shows the evaluation of the stepwise charge/discharge cycling performances for V_2O_5 nanowhiskers and the commercial V_2O_5 powders. It can be seen that the coral-like V_2O_5 nanowhiskers delivered the highest specific capacities at lower current rates, *e.g.* 0.05, 0.1 and 0.2 C with both CE and IL electrolytes, compared to commercial V_2O_5 powders. However, from 0.5 C, the capacities of the electrodes with the IL electrolyte degraded quickly, while the V_2O_5 nanowhisker electrode with the CE electrode still maintained high capacities at high rates. When the current rate reversed back to 0.1 C, the capacity of the V_2O_5 nanowhiskers with IL electrolyte recovered to 282 mAh g^{-1}.

To further evaluate the conductivity of battery cells with CE and IL electrolytes, alternating current (AC) impedance tests were performed at different working temperatures with an open circuit voltage of 3.4 V. Fig. 10 shows the electrochemical impedance spectra. The intercepts on the Z' axis at the high frequency region represent the resistance of the electrolyte (R_s) and the diameters of the semicircles on the spectra imply the charge transfer resistances (R_{ct}) at the electrolyte/electrode interface. It can be seen that, under all circumstances, lithium cells with both CE and IL electrolytes have quite low electrolyte resistance. However, both lithium cells with different filled-in electrolytes experienced significant decreases on the charge transfer resistance when the temperature was elevated from 20 °C to 50 °C. At room temperature (20 °C), the charge transfer resistance of the cell filled with IL electrolyte is much higher than that of cell with CE electrolyte. The differences in charge transfer resistance of these lithium cells were reduced significantly with increasing temperature. When the working

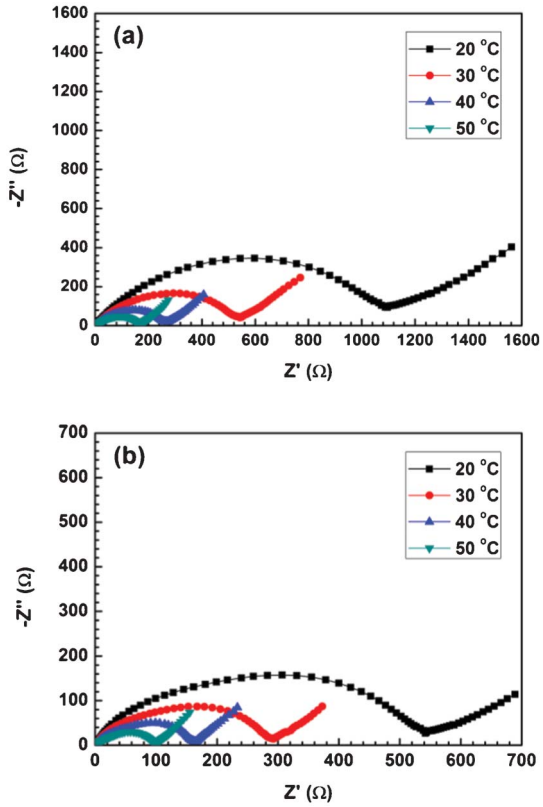

Fig. 10 Electrochemical impedance spectra of the V_2O_5 nanowhisker electrodes with electrolytes of (a) IL and (b) CE at elevated temperatures from 20, 30, 40 to 50 °C.

temperature was increased to 50 °C, the charge resistance in both cells became similar. This indicates similar capabilities of lithium diffusion in both cells at a working temperature of 50 °C.

For lithium cells filled with CE, excellent internal conductivity can be achieved, as presented in Fig. 10. Both V_2O_5 nanowhiskers and commercial powders were able to exhibit high specific capacities, as shown in Fig. 9, due to their small particle size in the nanometer scale. V_2O_5 nanowhisker electrode performed slightly better than V_2O_5 commercial powders, as a result of a higher BET surface area. On the other hand, when IL electrolyte was used, the assembled cells suffered from low ionic conductivity, as evidenced by AC impedance analysis. However, the larger contact area of the V_2O_5 nanowhisker sample can effectively buffer the drawback of the poor conductivity in the lithium cells. Therefore, V_2O_5 nanowhiskers can deliver higher capacities in IL than commercial powders at the same current rates.

To explore the possibility of rate performance improvement with the IL electrolyte, we tested the lithium cells at a working temperature of 50 °C. Electrodes of coral-like V_2O_5 nanowhiskers and commercial V_2O_5 powders were investigated with both CE and IL electrolytes. Fig. 11 shows their electrochemical properties in terms of specific capacity against cycle number at various current rates. Electrochemical perfor-

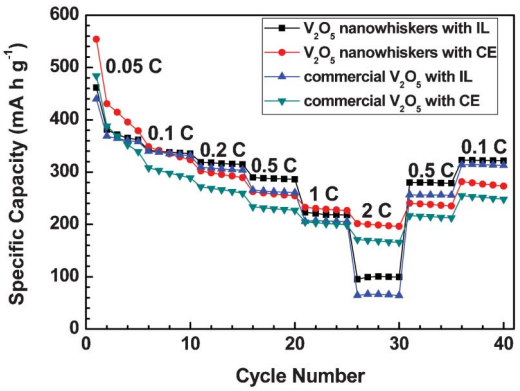

Fig. 11 Rate performances of V_2O_5 nanowhiskers and commercial V_2O_5 powders with both IL and CE at 50 °C.

mances of all electrodes were improved significantly with enhanced specific capacities and cycling stability with both CE and IL. In particular, V_2O_5 nanowhiskers with the IL electrolyte delivered specific capacities around 290 mAh g^{-1} at 0.5 C and 223 mAh g^{-1} at 1 C, which are several times higher than those at room temperature. The capacity retained around 323 mAh g^{-1} when the current rate reversed back to 0.1 C, showing excellent capacity retention. Lithium cells with a combination of V_2O_5 nanowhiskers and the IL electrolyte performed much better at high current rates at 50 °C, owing to the reduced charge transfer resistance.

In summary, with IL as the electrolyte, both V_2O_5 nanowhiskers and commercial powders showed excellent electrochemical properties at a low current rate (0.1 C); the V_2O_5 electrodes behaved much better in CE rather than IL at high current rates, as shown clearly in Fig. 9 and 11. The poor ionic conductivity of IL is the main reason for a poor rate performance of the prepared and commercial V_2O_5 materials. However, the rate performance of the cells with IL can be further improved at 50 °C as both the electrolyte and charge transfer resistances are further decreased. The overall electrochemical properties of V_2O_5 electrodes with IL, as reported in this work, reveal the possibility that CE could be replaced by IL at a low current rate or an increased working temperature for V_2O_5 nanowhisker cathode with comparable electrochemical performance. This offers IL further feasibility to be an applicable electrolyte as IL is able to retain more active material on the electrode and is much safer than CE in lithium-ion batteries.

Conclusions

Ultra-fine coral-like V_2O_5 nanowhiskers were prepared by a direct electrolytic method. The as-synthesized V_2O_5 nanowhiskers have a length of approximately 1 μm and a width of 50–60 nm. Significantly enhanced electrochemical properties of the as-prepared V_2O_5 nanowhiskers were achieved with an ionic liquid electrolyte (0.5 M $LiNTf_2$ in $[C_3mpyr][NTf_2]$). V_2O_5 nanowhiskers delivered a specific capacity of 461 mAh g^{-1} and an excellent cycling stability. The rate performance could be further improved at an elevated temperature of 50 °C, showing capacities of 290 mAh g^{-1} at 0.5 C and 223 mAh g^{-1} at 1 C. The combination of the V_2O_5 nanowhisker cathode materials and 0.5 M $LiNTf_2$ in $[C_3mpyr][NTf_2]$ ionic liquid electrolyte can achieve lithium-ion batteries with enhanced electrochemical performances at elevated temperatures.

Acknowledgements

The project is financially supported by the Australian Research Council (ARC) through the ARC Discovery Project (DP1093855).

Notes and references

1 D. Lindley, *Nature*, 2010, **463**, 18–20.
2 Q. Schiermeier, J. Tollefson, T. Scully, A. Witze and O. Morton, *Nature*, 2008, **454**, 816–823.
3 A. S. Arico, P. Bruce, B. Scrosati, J. M. Tarascon and W. Van Schalkwijk, *Nat. Mater.*, 2005, **4**, 366–377.
4 P. Poizot, S. Laruelle, S. Grugeon, L. Dupont and J. M. Tarascon, *Nature*, 2000, **407**, 496–499.
5 J. M. Tarascon and M. Armand, *Nature*, 2001, **414**, 359–367.
6 G. Wang, H. Liu, J. Liu, S. Qiao, G. M. Lu, P. Munroe and H. Ahn, *Adv. Mater.*, 2010, **22**, 4944–4948.
7 Y. Wang and G. Cao, *Adv. Mater.*, 2008, **20**, 2251–2269.
8 N. Jayaprakash, J. Shen, S. S. Moganty, A. Corona and L. A. Archer, *Angew. Chem. Int. Ed.*, 2011, **50**, 5904–5908.
9 X. Ji, S. Evers, R. Black and L. F. Nazar, *Nat. Commun.*, 2011, **2**, 325.
10 X. Ji, K. T. Lee and L. F. Nazar, *Nat. Mater.*, 2009, **8**, 500–506.
11 Y. Wang and G. Z. Cao, *Chem. Mater.*, 2006, **18**, 2787–2804.
12 S. L. Chou, J. Z. Wang, J. Z. Sun, D. Wexler, M. Forsyth, H. K. Liu, D. R. MacFarlane and S. X. Dou, *Chem. Mater.*, 2008, **20**, 7044–7051.
13 H. X. Li, L. F. Jiao, H. T. Yuan, M. Zhang, J. Guo, L. Q. Wang, M. Zhao and Y. M. Wang, *Electrochem. Commun.*, 2006, **8**, 1693–1698.
14 Y. Wang, K. Takahashi, H. M. Shang and G. Z. Cao, *J. Phys. Chem. B*, 2005, **109**, 3085–3088.
15 Y. Wang, K. Takahashi, K. Lee and G. Z. Cao, *Adv. Funct. Mater.*, 2006, **16**, 1133–1144.
16 B. X. Li, Y. Xu, G. X. Rong, M. Jing and Y. Xie, *Nanotechnology*, 2006, **17**, 2560–2566.
17 A. M. Cao, J. S. Hu, H. P. Liang and L. J. Wan, *Angew. Chem. Int. Ed.*, 2005, **44**, 4391–4395.
18 P. Liu, S. H. Lee, C. E. Tracy, Y. F. Yan and J. A. Turner, *Adv. Mater.*, 2002, **14**, 27–30.
19 E. Potiron, A. L. La Salle, S. Sarciaux, Y. Piffard and D. Guyomard, *J. Power Sources*, 1999, **81**, 666–669.
20 E. Potiron, A. L. La Salle, A. Verbaere, Y. Piffard and D. Guyomard, *Electrochim. Acta*, 1999, **45**, 197–214.
21 E. Shembel, R. Apostolova, V. Nagirny, D. Aurbach and B. Markovsky, *J. Power Sources*, 1999, **81**, 480–486.

22 C. Delmas, S. Brèthes and M. Ménétrier, *J. Power Sources*, 1991, **34**, 113–118.
23 C. Delmas, H. Cognacauradou, J. M. Cocciantelli, M. Menetrier and J. P. Doumerc, *Solid State Ionics*, 1994, **69**, 257–264.
24 N. Byrne, P. C. Howlett, D. R. MacFarlane and M. Forsyth, *Adv. Mater.*, 2005, **17**, 2497–2501.
25 M. Galiński, A. Lewandowski and I. Stępniak, *Electrochim. Acta*, 2006, **51**, 5567–5580.
26 C. Peng, L. Yang, Z. Zhang, K. Tachibana and Y. Yang, *J. Power Sources*, 2007, **173**, 510–517.

RSC Publishing

Publishing

RSC Advances

An international journal to further the chemical sciences

About RSC Advances

Scope
RSC Advances is an international, peer-reviewed, online journal covering all of the chemical sciences, including multidisciplinary and emerging areas. Main research areas include (but are not limited to):

Agricultural
Analytical
Biochemistry
Biological
Biophysics
Biotechnology
Catalysis
Chemical Biology
Chemical Engineering
Computational Chemistry
Coordination chemistry
Electrochemistry
Energy
Environmental Sciences
Food
Genetic engineering
Geochemistry
Green chemistry
Inorganic
Ionic Liquids
Kinetics
Materials
Medicinal
Microarrays
Nanomedicine
Nanoscience
Neurochemistry
Nucleic Acids
Organic
Organometallics
Pharmacology
Pharmaceutics
Photosciences
Physical
Polymers
Protein engineering
Proteomics
Rheology and colloids
Sensors and Biosensors
Supramolecular
Surfaces
Synthetic Biology
Theoretical Chemistry
Toxicology

The criteria for publication are that the work must be high quality and well conducted. Articles submitted to the journal will be evaluated by international referees for the overall quality and accuracy of the science presented.

Why Publish with *RSC Advances*?
RSC journals are renowned for their high quality, rapid publication and innovative technology. All articles published in *RSC Advances* will benefit from wide exposure, with the Journal indexed in all major databases including ISI and Scopus.

RSC Advances authors will benefit from:

- Rapid publication times
- Open-access options
- Simple and effective online submission process
- Free electronic reprints (pdf) of own paper
- Free use of colour
- No page charges
- No page limits

In addition, all articles published in *RSC Advances* will be discovered within and/or between disciplines

through our innovative and sophisticated behind-the-scenes **topic modelling**. Content will be automatically classified into one or more of the twelve main subject categories on the *RSC Advances* website giving maximum visibility to your work.

Article Types
RSC Advances publishes communications, papers and reviews.

Readership
Academic, government and industrial scientists from all disciplines- specialised or interdisciplinary including: organic, medicinal, inorganic, organometallic, physical and biochemists, biologists, physicists, engineers, theoretical chemists; analytical, materials, polymer, surface, sustainable energy and environmental scientists.

RSC Advances readers benefit from:

- Enhanced browsing and searching functionality online
- Free access to all *RSC Advances* articles published in volumes 1 and 2
- Free e-mail alerting and RSS news feeds service

Related Links

Submit your work today
Submit your work to RSC Advances

External links will open in a new browser window